Construction and Building Materials 472 (2025) 140867

Contents lists available at ScienceDirect

Construction and Building Materials

journal homepage: www.elsevier.com/locate/conbuildmat

Fire resistance and thermal performance of hybrid fibre-reinforced magnesium oxychloride cement-based composites

Farhan Ahmad [a], S. Rawat [a], Richard (Chunhui) Yang [a], Lihai Zhang [b], Y.X. Zhang [a,*]

[a] Centre for Advanced Manufacturing Technology, School of Engineering, Design and Built Environment, Western Sydney University, NSW 2751, Australia
[b] School of Infrastructure Engineering, The University of Melbourne, VIC 3010, Australia

ARTICLE INFO

Keywords:
Fire resistance
Hybrid fibre
Magnesium oxychloride cement
Residual strength
Thermal performance

ABSTRACT

Magnesium oxychloride cement (MOC) is recognized as an eco-friendly alternative to Ordinary Portland Cement (OPC) with inherent fire resistance. However, its thermal and mechanical performance under fire and the underlying fire resistance mechanisms have not been well understood. This study examines the fire resistance and thermal performance of hybrid polyethylene (PE) and basalt fibre (BF) reinforced MOC-based composite (HFMOC) modified with ground granulated blast furnace slag (GGBFS) and metakaolin (MK), which was designed and developed to enhance the fire resistance capacity of HFMOC especially for non-structural application such as cladding. The compressive and tensile strength tests were conducted at elevated temperatures (200°C–800°C and 200°C–600°C, respectively) and the results revealed a significant strength reduction exceeding 90 % at 600°C. Moreover, the composite exhibited excellent resistance to spalling, good insulating properties, and non-combustibility, making it suitable for non-structural applications where residual strength is less critical. XRD analysis indicated that the reduction in strength at elevated temperatures was associated with the continuous degradation of the main hydration product, phase 5, which was entirely converted to MgO before 600°C. Morphological analysis verified the findings from XRD showing a weak and porous interfacial transition zone at elevated temperatures caused by the loss of crystalline phases, which was further supported by DSC analysis showing a mass loss of 36–38.1 %.

1. Introduction

Fire hazards are considered as one of the most serious risks, making fire resistance a crucial factor in designing civil engineering infrastructure such as buildings. For high-rise buildings fire often starts from claddings largely attributed to the use of combustible cladding materials which facilitated fire propagation [1], posing significant risks to occupants. Specifically in Australia, Governments have instituted stringent guidelines to mitigate the risk of cladding-related fire incidents [2,3], and recent regulations prohibit the use of certain aluminium composite panels on specific building types. These underscore the urgent need for developing alternative and durable construction and building materials, especially for claddings [4]. Research efforts have been made to develop cladding materials that are sustainable, durable, lightweight, non-combustible, energy-efficient, and cost-effective [5–7]. Several studies have explored different cladding materials, yet each has its pros and cons. Claddings made from concrete, stone, and brick impose significant weight on buildings due to their extensive surface coverage [8]. Aluminium has lower density compared to these traditional materials, but the high cost of aluminium is prohibitive. Timber, although green and light, faces durability issues [9]. Plastics, though light in weight, pose significant environmental and flammability challenges, while the brittleness of glass raises concerns about structural integrity and safety [10]. These challenges highlight the need to develop alternative cladding material, which is green, light, and cost effective with sufficient thermal resistance to meet energy efficiency standards in building construction.

Magnesium oxychloride cement (MOC) has emerged as a prominent choice for cladding materials owing to its advantageous properties [11]. MOC is recognized as an eco-friendly alternative to Ordinary Portland Cement (OPC), offering several superior characteristics, including low energy demand and low carbon emissions during manufacturing, lightweight, low thermal conductivity, and fire resistance [12,13]. Unlike OPC (pH 12–13), MOC has a comparatively lower pH of 10–11,

* Corresponding author.
E-mail addresses: f.ahmad@westernsydney.edu.au (F. Ahmad), sanket.rawat@uts.edu.au (S. Rawat), R.Yang@westernsydney.edu.au (R.(C. Yang), lihzhang@unimelb.edu.au (L. Zhang), Sarah.Zhang@westernsydney.edu.au (Y.X. Zhang).

https://doi.org/10.1016/j.conbuildmat.2025.140867
Received 7 January 2025; Received in revised form 2 March 2025; Accepted 13 March 2025
Available online 24 March 2025

making it more suitable for commonly used fibres such as polyvinyl alcohol fibres, glass fibres, BF, and PE fibres, without the risk of aging-related degradation [14]. Additionally, MOC exhibits strong bonding with various industrial by-products, including marble powder, wood particles, sewage sludge ash, fly ash, phosphogypsum, granite powder, slag, and expanded clay [15]. Furthermore, the recent developments of water-resistant MOC [16,17] and ductile fibre-reinforced MOC [15,18,19] broaden its scope of applications from indoor to outdoor where durability has been a prime concern. These remarkable attributes make MOC an attractive option for developing fire-resistive cladding materials, prompting urgent needs for further research into its thermal and fire performance.

MOC has generally been regarded as inherently fire-resistant [19,20], however, limited studies have explored its fire performance and thermal properties, and a thorough understanding of the underlying mechanisms remains lacking. Early studies by Montle et al. [21] and Thompson et al. [22] evaluated MOC as a fire-resistant coating material, highlighting its excellent insulating properties. These studies attributed MOC's excellent thermal resistance to the abundance of crystalline water and MgO (melting point > 2800°C), which effectively reflects heat and acts as an insulator and fire retardant when applied as a coating agent. However, few investigations have explored MOC's thermal performance as a construction material. Chang et al. [23] examined the mechanical characteristics of pure MOC at elevated temperatures, noting a complete loss in compressive and flexural strength as temperatures increased from 10 to 500°C. Similarly, Rawat et al. [24] reported a 90 % and 97.8 % loss in compressive strength of MOC at 600°C and 800°C, respectively, attributing the reduction to substantial mass loss of 34.8 %. Ahmad et al. [25] found compressive strength almost negligible at 800°C, with a mass loss of approximately 36.0 %. More recently, Rawat et al. [11] sought to enhance MOC's mechanical performance at elevated temperatures by incorporating hybrid fibres such as basalt fibre (BF), polypropylene (PP) fibre, and fly ash. Despite a significant decline in compressive strength exceeding 95 % at 800°C, the study observed minimal cracking and no spalling, suggesting MOC's potential as a fire-resistant cladding material for non-structural applications. The compressive strength retention was improved compared to the mix proposed by Chang et al. [23] attributed to the inclusion of fly ash and hybrid fibres. They recommended further research into incorporating different mineral admixtures in MOC to develop hydration phases with greater thermal stability.

In recent years, various supplementary cementitious materials (SCMs) such as fly ash, GGBFS, and MK, have been incorporated to enhance the residual mechanical performance of OPC-based composites at elevated temperatures highlighting the pronounced effect of these industrial by-products [26,27]. Compared to other SCMs, GGBFS has been found to be particularly effective, significantly improving residual strength characteristics at elevated temperatures [28], as also demonstrated by Rawat et al. [29]. It was found that substituting OPC with high-volume GGBFS resulted in strength retention of approximately 75 % at 600°C and 45 % at 800°C. Fly ash-modified composites have also been found to be able to improve strength retention compared to pure OPC-based composites [30]; however, the global shift from coal-fired thermal power plants to renewable energy sources has resulted in a scarcity of fly ash [31]. Regarding the performance of MK-modified composites at elevated temperatures, Abdelmelek et al. [32] showed that composites containing 9 % MK retained approximately 56 % of their strength at 800°C, with no spalling and only minimal surface cracking. Furthermore, Albidah et al. [33] and Nabil et al. [34] also reported enhanced performance of MK-modified cementitious composites at elevated temperatures. The global availability of GGBFS and MK, coupled with their enhanced performance in OPC-based composites at elevated temperatures, makes them suitable candidates for improving the performance of MOC-based composites at elevated temperatures.

Additionally, past studies have demonstrated that incorporating hybrid fibres containing both low- and high-melting point fibres effectively enhances the thermal performance of cementitious composites [27]. Low melting point fibres, such as polyethylene (PE), PP, or polyvinyl alcohol (PVA) fibre enhance spalling resistance by melting under thermal exposure and creating porous channels that facilitate internal vapour pressure release [35]. In contrast, high melting point fibres such as steel fibre or BF help maintain the structural integrity of specimens at elevated temperatures [11,36]. Recently, Ahmad et al. [18] investigated the compressive and tensile behaviour of MOC composites reinforced with 1.25 % PE and 0.75 % BF, along with 30 % fly ash, and found improved compressive strength (78.8 MPa), tensile strength (8.49 MPa), and strain capacity (2.43 %). In this study, a hybrid fibre combination containing low melting point PE fibre and high melting point BF was selected based on its excellent strength, ductility, and fire performance, as recommended by published research [15,18,27,37].

This study aims to develop a sustainable, fire-resistant, and non-combustible MOC based hybrid fibre reinforced cementitious composite (HFMOC) modified with GGBFS, MK, and hybrid GGBFS-MK for non-structural applications such as cladding. Hitherto, no prior research has evaluated the residual strength, non-combustibility, and thermal performance of the HFMOC. Mass loss and visual inspections including spalling resistance, colour change, and surface cracking, were examined post-fire exposure. Additionally, thermal conductivity and non-combustibility analysis of HFMOC were conducted to analyse the insulation behaviour at varying temperatures (20°C–500°C) and non-combustible nature, respectively. The compressive and tensile strengths were also evaluated at different temperature ranges from 200–800°C and 200–600°C, respectively to assess its residual strength. Detailed microstructural and materials characterisation analyses, including SEM, XRD, and DSC, were conducted to explore the underlying mechanisms affecting the composites at varying temperatures.

2. Experimental programs

2.1. Materials and mix proportions

In this study, materials utilized for the development of the HFMOC included MgO (95 % purity), GGBFS, MK, local river sand (passing through 300 μm sieve), magnesium chloride hexahydrate ($MgCl_2.6H_2O$) (99 % purity) dissolved in normal tap water, phosphoric acid (PA) (85 %), sodium monofluorophosphate (MFP) (95 %), and ADVA LS780-based high-range water reducer (HRWR). The characteristics such as morphology, phase composition, and elemental analysis of the raw materials, along with their sources, were presented in the previous work of the authors [18]. Table 1 shows the mineral oxide composition of the raw materials including GGBFS, MK and MgO obtained from X-ray fluorescence analysis (XRF) analysis. BF (12 mm length, 13 μm diameter, 2.65 g/cm^3 density, 91–110 GPa elastic modulus) and PE fibre (12 mm length, 24 μm diameter, 0.97 g/cm^3 density, 116 GPa elastic modulus) were used to reinforce the matrix to form the HFMOC.

Table 2 illustrates the detailed mix proportions of the HFMOC,

Table 1
Chemical analysis of raw materials (wt%).

Chemical compositions (%)	GGBFS	MK	MgO
Al_2O_3	14.6	48.6	0.11
SiO_2	33.7	49.5	1.32
SO_3	2.33	_	_
K_2O	0.36	0.09	_
MgO	8.17	_	95.2
CaO	39.6	0.19	2.95
TiO_2	0.46	0.97	_
MnO	0.15	_	0.11
Fe_2O_3	0.23	0.41	0.17
Cl	_	_	_
Trace elements	0.40	0.24	0.14

Table 2
Details of HFMOC mix proportions.

Mix ID	M	H	S/B	GGBFS (wt%)	MK (wt%)	PA (wt%)	MFP (wt%)	PE (vol%)	BF (vol%)
G30	9	13	0.23	30	_	0.5	0.5	1.25	0.75
M30	9	13	0.23	_	30	0.5	0.5	1.25	0.75
G15M15	9	13	0.23	15	15	0.5	0.5	1.25	0.75

adopted from the authors' previous study [15]. Three different mixes were prepared with varying GGBFS and MK contents while keeping other components constant to assess their effects on HFMOC. The mixes include G30 (30 % GGBFS), M30 (30 % MK), and G15M15 (15 % GGBFS + 15 % MK). The MOC mix formulation, with a molar ratio of $MgO/MgCl_2$ (M):9-$H_2O/MgCl_2$ (H):13, along with 0.5 % phosphoric acid (PA) and 0.5 % sodium monofluorophosphate (MFP), was based on the authors' earlier research [38]. A sand-to-binder (S/B) ratio of 0.23 was maintained. The optimal fibre dosage, consisting of 1.25 % PE and 0.75 % BF, was selected for its superior compressive strength (78.8 MPa), tensile strength (8.49 MPa), and ultimate tensile strain capacity (2.43 %) in MOC-based composites, as recommended by Ahmad et al. [18].

2.2. Mixing procedures and specimen preparation

Fig. 1 depicts the detailed mixing technique of HFMOC as adopted from previous research [18]. Initially, the concentrated $MgCl_2$ solution, HRWR, PA, and MFP were mixed via a hand blender followed by dry mixing of MgO, sand, GGBFS, and MK using a shear mixer. Subsequently, the wet mixing was done by blending the prepared solution with the dry powder mix followed by adding fibres. Ultimately, the resultant mixture was utilized to fill appropriate molds for each test. Cubical specimens (50 mm), cuboid specimens (50 mm × 50 mm × 20 mm), cylindrical specimens (50 mm height and 45 mm diameter), and dog bone specimens (340 mm length × 50 mm width × 13 mm thickness) were cast to evaluate compressive strength, thermal conductivity, non-combustibility, and tensile strength, respectively. The molds were covered with polyethylene sheets to prevent surface dehydration, and specimens were demolded after 24 hours. Finally, specimens were cured in a chamber under controlled conditions (25 ± 2°C ambient temperature and 65 ± 5 % relative humidity) until the testing date.

3. Test procedures

Fig. 2 presents the schematic representation of the comprehensive experimental plan employed in this study. Initially, the procedures for the hot disk test and non-combustibility test are explained. Subsequently, the method for evaluating the mechanical properties of HFMOC at elevated temperatures is described. Finally, the detailed micro-testing and material characterization procedures are given.

3.1. Visual inspection and mass loss

Visual inspection was conducted pre- and post-heating to identify any physical changes or damage. Key observations included spalling behaviour, cracking, colour change, and surface conditions such as

Fig. 1. Mixing procedures of HFMOC.

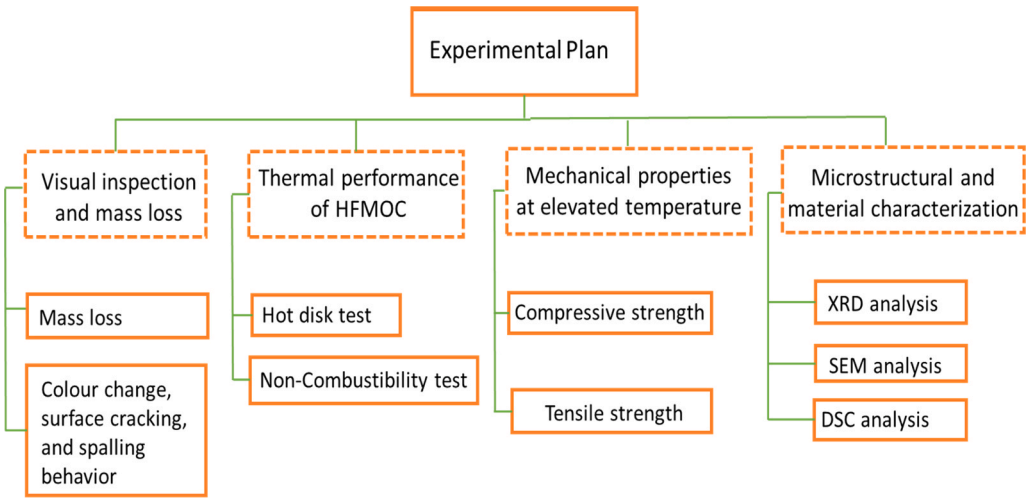

Fig. 2. Detailed experimental plan of HFMOC.

roughness or texture changes. Colour change provided insights into chemical changes or material degradation, while surface cracking visualization offered information about cracks' presence, pattern, and severity. Mass loss for HFMOC specimens was measured using an analytical balance by determining the difference in mass between ambient temperature (M_0) and each exposed temperature (M_t) as shown in Eq. 1.

$$\text{Mass loss}(\%) = \left(\frac{M_0 - M_t}{M_0}\right) \times 100 \quad (1)$$

3.2. Thermal performance of HFMOC

3.2.1. Thermal conductivity test

Thermal conductivity is crucial for assessing thermal performance, insulation capabilities, and fire resistance for cementitious composites and its suitability for applications across construction and engineering sectors. A Hot Disk TPS 2500 S was used to measure the thermal conductivity of HFMOC both at ambient and elevated temperatures. Specimens with dimensions of 50 mm × 50 mm × 20 mm were tested. At ambient temperature, a Kapton 5501 sensor with an extended grey cable was used. For evaluations at elevated temperatures up to 500°C, a Mica 5082 sensor with a four-point probe macro sensor holder installed inside the furnace was utilized. The measurement time was set to 80 seconds, and the heating power was 0.1 W.

3.2.2. Non-combustibility test

The non-combustibility test of HFMOC was conducted according to AS 1530.1 [39] using a tube furnace with a cone-shaped airflow

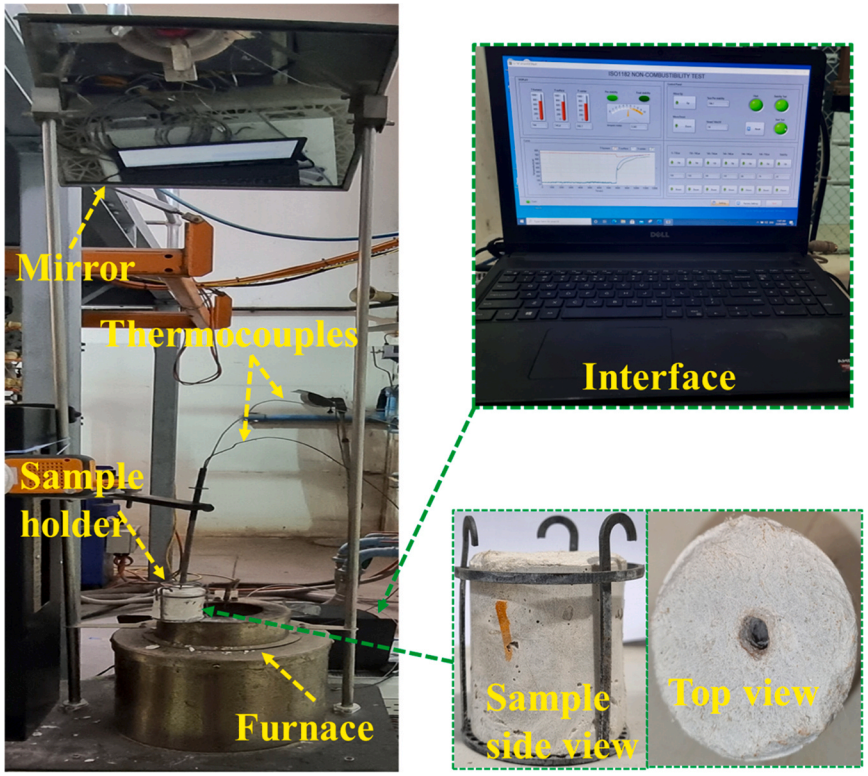

Fig. 3. Non-combustibility test setup.

stabilizer (Fig. 3). Cylindrical specimens (50 mm height, 45 mm diameter) with a 2 mm central hole for thermocouple installation were prepared. Three K-type thermocouples were used to measure temperature variations at the specimen centre, surface, and furnace wall. The furnace was first stabilized at 750 ± 5°C, ensuring a temperature drift of no more than 2°C in 10 minutes. Once stabilized, the specimen with its holder was inserted, and the appearance and duration of sustained flames were recorded by visualizing the mirror at the furnace head. The test continued until the thermocouples reached equilibrium (temperature change ≤ 2°C over 10 minutes) after 30 minutes. If not, the test continued until the criteria were met as per AS 1530.1 [39]. After testing, the specimen was cooled to room temperature, and its residual mass was measured.

3.3. Mechanical properties of HFMOC at elevated temperatures

The mechanical properties including compressive and tensile strengths of 28-day cured HFMOC specimens, were evaluated at ambient and elevated temperatures. For compressive strength evaluation, cubical specimens were assessed using an Instron compressive testing machine with a 3000 kN loading capacity and a constant loading rate of 20 MPa/min. For uniaxial tensile strength measurement, dog bone specimens with a gauge length of 60 mm and a cross-sectional area of 30 mm × 13 mm (reduced section) were tested using an Instron tensile testing machine with a 250 kN loading capacity at a uniform displacement-controlled loading rate of 0.1 mm/min. Two linear variable displacement transducers (LVDTs) were attached to both sides of the sample using a steel rig to record displacement, as illustrated in Fig. 4a. The specimens were heated in a muffle furnace (Fig. 4b) at a heating rate of 2 °C/min, with a withholding period of 2 hours (hrs) at each peak temperature, based on parameters found suitable for isothermal heating according to previous literature [27]. Cubical specimens were exposed to 200, 400, 600, and 800°C temperatures, while dog bone specimens were subjected to 200, 400, and 600°C. After exposure, the specimens were allowed to cool naturally inside the furnace for 24 hrs before conducting compressive or tensile testing to evaluate their residual performance.

3.4. Microstructural and material characterization

The developed HFMOC was characterized using SEM, XRD, and DSC analyses (Fig. 5). These analyses provided insights into the variations in morphology, phase changes, and decomposition of crystalline phases with increasing temperatures, elucidating the underlying mechanisms affecting the residual strength characteristics. The analysis was conducted on specimens subjected to compression testing. Samples were collected from the core of the crushed specimens and soaked in ethanol for 48 hours to halt hydration. Parts of the samples were then powdered for XRD and DSC analyses, with the remaining solid portion utilized for SEM analysis. Phenom XL SEM was employed to analyse the morphology of the carbon-coated solid samples under test conditions of 15 kV accelerating voltage and 1 Pa chamber pressure. The crystalline phases were examined using XRD analysis with Cu Kα radiation. The analysis was carried out using a Bruker D8 Advance XRD analyser, with scans performed across a 2θ range of 5° to 80° at a scanning rate of 0.2°/min. DSC analysis was performed using "NETZSCH STA 449F3", where the thermal decomposition of hydration phases was investigated within the temperature range of 35–800°C, with a heating rate of 10 °C/min. This analysis effectively captured the stepwise thermal degradation of the crystalline phases.

4. Results and discussion

4.1. Visual inspection

A visual inspection of specimens after thermal exposure can serve as a preliminary assessment of thermal performance. Fig. 6 depicts the variations in the exterior surfaces of the HFMOC specimens subjected to different temperatures regarding their colour change, spalling, and crack formation. No spalling failure was observed, as evident from the surface appearance of HFMOC specimens at different temperatures. This can be attributed to the presence of PE fibre and BF. The PE fibre prevents spalling at lower temperatures, typically melting at around 150°C, creating pores or channels inside the composites that facilitate the release of internal vapor pressure [27]. Meanwhile, the presence of BF maintains the integrity of the specimens at higher temperatures and prevents spalling through bridging action [37].

Fig. 6 shows the colour changes of HFMOC specimens with increasing temperature. Initially grey at ambient temperature, the specimens became lighter grey at 400°C and transformed to a completely whitish appearance at 800°C. This whitish appearance at 800°C is attributed to the significant degradation of the matrix, resulting in the formation of residual MgO, which is typically white and a by-product at this temperature [11]. Up to 400°C, no cracking was

Fig. 4. (a) Instron tensile testing setup and (b) muffle furnace.

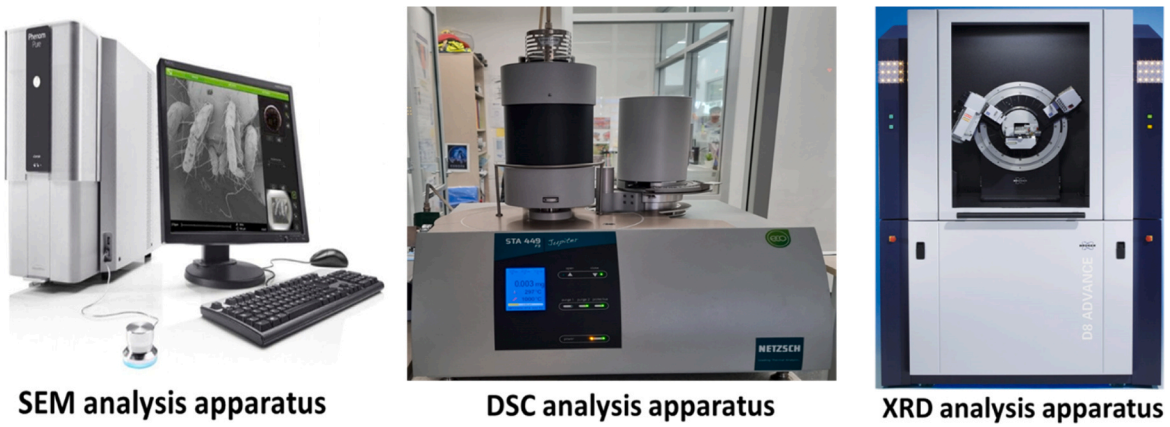

Fig. 5. Testing setup used for microstructural analysis.

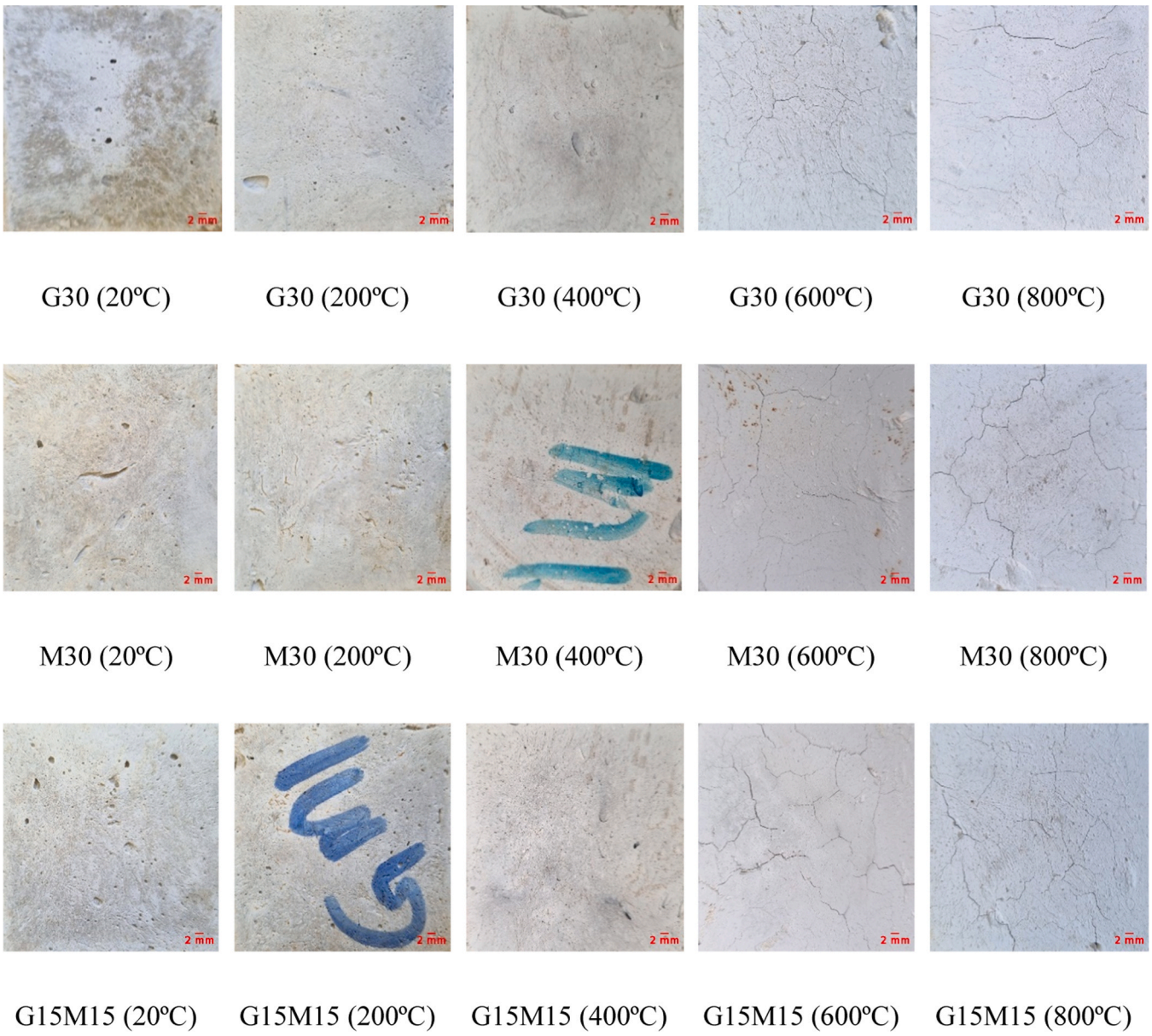

Fig. 6. Variation in surface appearance of HFMOC at elevated temperatures.

observed, followed by minor cracking at 600°C. At 800°C, the cracks were slightly wider compared to those at 600°C. The absence of cracks at lower temperatures is likely due to the presence of low melting point PE fibres, which facilitate the release of internal vapor pressure and gases without affecting the specimen's integrity [27]. Minor cracks at higher temperatures can be attributed to the complete decomposition of hydration products, leading to a porous interfacial transition zone (ITZ). However, the presence of BF maintained the specimen's integrity at elevated temperatures, preventing spalling and overall damage [37]. The enhanced spalling resistance of HFMOC specimens at elevated temperatures highlights the potential of MOC for non-structural applications such as cladding and facades.

4.2. Mass loss of HFMOC

Fig. 7 illustrates the mass loss obtained from the pre- and post-exposure of cubical HFMOC specimens at different temperatures. An approximately similar incremental trend of mass loss for all HFMOC can be seen with the rising temperature. The minor differences in mass loss corresponding to each temperature could be attributed to the presence of different mineral admixtures and the stability of hydration products. However, the overall mass loss difference corresponding to each temperature was not significant. The mass loss reported at 200ºC ranged from 5 % to 6.56 %, followed by 20–22.0 %, 34–35.4 %, and 36–38.1 % corresponding to 400, 600, and 800ºC. Unlike conventional concrete and fibre-reinforced cementitious composites where mass loss is usually dominant up to 400ºC, beyond that temperature, the loss occurs at a comparatively modest rate, resulting in an overall mass loss ranging from 17–20 % [27,40].

The mass loss of cementitious composites is primarily due to the loss of absorbed water, free water, and chemically bound water through evaporation, closely associated with the degradation of hydrated compounds. In terms of hydrated products, HFMOC significantly differs from OPC-based composites, resulting in unique patterns of mass loss. This can be attributed to the presence of different temperature-sensitive hydration products in MOC, influencing mass loss. For instance, phase 5, the major hydration product of MOC, begins degrading and destabilizing nearly at 100°C, followed by complete degradation up to 500°C as illustrated in Eqs. 2–5 [11,38]. Beyond 350°C, brucite ($Mg(OH)_2$) begins to degrade until it is fully decomposed, regenerating light white MgO as a by-product. Additionally, the decomposition of carbonate phases starts beyond 500°C, further contributing to mass loss. These changes indicate that elevated temperatures significantly impact HFMOC, resulting in considerable mass loss in the form of moisture. This adversely affects the mechanical properties of HFMOC, yet it underscores the composite's potential as a fire-retardant. The presence of high melting point MgO particles (>2800°C), together with substantial moisture release, enables the composite to effectively reflect heat without compromising its structural integrity [19].

$$5Mg(OH)_2{\cdot}MgCl_2{\cdot}8H_2O \rightarrow 5Mg(OH)_2{\cdot}MgCl_2{\cdot}4H_2O + 4H_2O \quad (40°C–110°C) \tag{2}$$

$$5Mg(OH)_2{\cdot}MgCl_2{\cdot}4H_2O \rightarrow 5Mg(OH)_2{\cdot}MgCl_2 + 4H_2O \ (100°C–230°C) \tag{3}$$

$$5Mg(OH)_2{\cdot}MgCl_2 \rightarrow MgCl_2{\cdot}H_2O_{+4H2O} + 5MgO \ (350°C–500°C) \tag{4}$$

$$MgCl_2{\cdot}H_2O \rightarrow MgO + 2HCl \ (350°C–500°C) \tag{5}$$

$$MgCO_3 \rightarrow MgO + CO_2 \ (500°C–800°C) \tag{6}$$

4.3. Thermal performance of HFMOC

4.3.1. Thermal conductivity

In general, materials with lower thermal conductivity tend to offer better insulation capabilities. Fig. 8 illustrates the thermal conductivity of the HFMOC specimens across temperatures from 20ºC to 500ºC. At ambient temperature, the HFMOC with a denser microstructure shows higher thermal conductivity, likely due to its lower porosity. As the temperature increases, all HFMOC specimens demonstrate a consistent decline in thermal conductivity. This reduction is attributed to increased porosity caused by water evaporation and the melting of PE fibres at higher temperatures [27]. Among the specimens, G30 exhibited the highest thermal conductivity at ambient temperature, followed by M30 and G15M15. However, G30 also experienced a more significant decrease in thermal conductivity with rising temperatures.

At ambient temperature, the thermal conductivities of G30, M30, and G15M15 were 1.30, 1.19, and 1.16 W/(m.K), respectively. The higher thermal conductivity of G30 is attributed to its denser matrix at the ITZ compared to M30 and G15M15. A significant drop in thermal conductivity was observed for all HFMOC specimens when the temperature increased to 100ºC, with a gradual decline continuing up to 500ºC, as shown in Fig. 8. At 100ºC, the thermal conductivity decreased by approximately 56.0 %, 55.1 %, and 50.6 % for G30, M30, and G15M15, respectively. The reduction at higher temperatures ranged from 62.9 % to 73.4 % at 200ºC, 71.4–81.9 % at 300ºC, 78.3–85.6 % at 400ºC, and 83.5–89.3 % at 500ºC. G30 exhibited the highest reduction of about 89.3 % at 500ºC, compared to 85.5 % for M30 and 83.5 % for G15M15. This reduction in thermal conductivity with increasing temperature can be explained by the phonon hypothesis [41], which suggests that heat conduction occurs through phonons. At higher temperatures, phonons move more vigorously, leading to increased heat loss, and consequently, a reduction in thermal conductivity. Additionally, the evaporation of free and crystalline water and melting of PE fibre

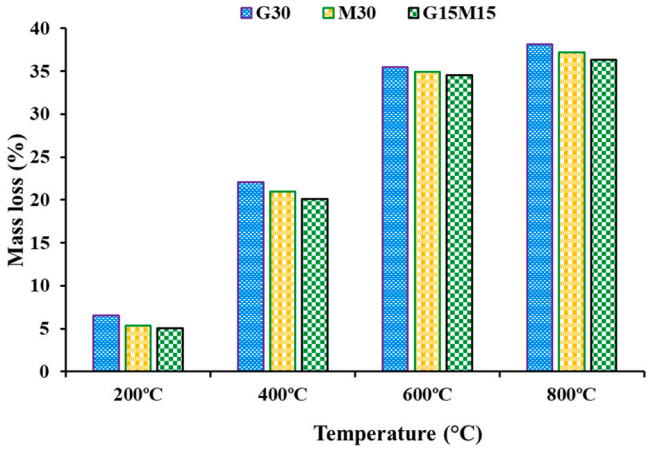

Fig. 7. Mass loss of HFMOC at elevated temperatures.

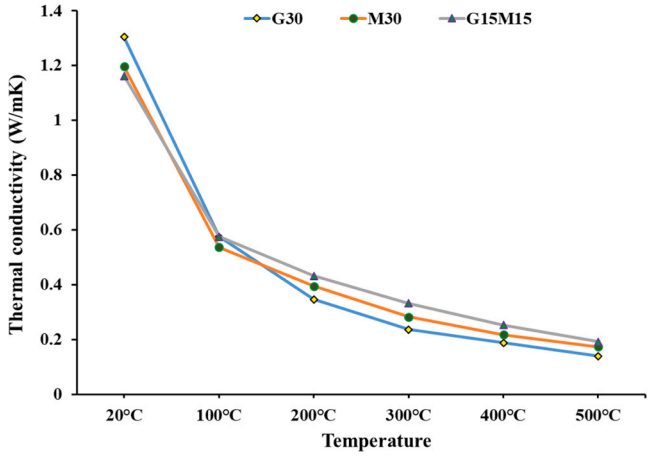

Fig. 8. Thermal conductivity of HFMOC at varying temperatures.

increased the porosity of the matrix, contributing to reduced thermal conductivity at elevated temperatures [27]. The thermal conductivity of HFMOC is comparatively lower than that of lightweight and normal-weight OPC-based composites (1.32–2.25 W/(m.K)) [27,42–45] and other cementitious materials reported in previous studies [46–48]. Overall, the lower thermal conductivity of HFMOC specimens at both ambient and high temperatures indicates that HFMOC is a promising material for thermal insulation, consistent with the excellent insulation capabilities of cement-based materials reported in previous studies [27, 41,49,50].

4.3.2. Non-combustibility

The non-combustibility of building materials is essential to ensure the fire safety and protection of infrastructures. For the non-combustibility test, both AS 1530.1 [39] and ASTM E2652 [51] follow a similar procedure, but differ in evaluation criteria, as outlined in Table 3. As per AS 1530.1, a material is considered combustible if it exhibits sustained flaming for 5 seconds or more. In contrast, ASTM E2652 considers a material combustible if the sustained flaming duration exceeds 10 seconds. This indicates that AS 1530.1 is more stringent than ASTM E2652 in terms of the duration of sustained flaming. Additionally, ASTM E2652 includes a mass loss requirement, specifying that a material should not lose more than 50 % of its mass to be considered non-combustible. The non-combustibility test results for the different HFMOC specimens are illustrated in Table 3. The results showed no sustained flaming for any of the specimens, demonstrating their non-flammable nature. Furthermore, the observed mass loss for the different HFMOC specimens ranged from 37.5 % to 40.2 %, which is well below the 50 % threshold. Overall, it can be concluded that all HFMOC specimens are non-combustible as per AS 1530.1 and ASTM E2652.

4.4. Mechanical properties of HFMOC at elevated temperatures

4.4.1. Compressive strength

Fig. 9 illustrates the variation in compressive strength and normalized residual compressive strength of HFMOC at elevated temperatures. The results reveal that G30 exhibited the highest compressive strength followed by M30 and G15M15 at room temperature. A substantial decline in compressive strength was observed with rising temperature. A gradual drop in strength was noted up to 200°C, followed by a steep decline at 400°C and 600°C. The compressive strengths at 600°C and 800°C were approximately identical, indicating a substantial loss in strength.

G30 containing 30 % GGBFS exhibited approximately 7.58 % and 9.20 % higher compressive strength than M30 and G15M15, respectively at room temperature. Meanwhile, M30 with 30 % metakaolin showed approximately 1.76 % higher strength than G15M15 but was 8.12 % lower than G30. The strength development in all HFMOC mixes was primarily driven by the formation of phase 5 crystals ($5Mg(OH)_2{\cdot}MgCl_2{\cdot}8\,H_2O$). The SCM contributed to better dispersion of MgO and entrapped water during mixing, which, upon release, facilitated the hydration of unreacted MgO and promoted phase 5 formation [52,53]. Additionally, the inclusion of 30 % GGBFS had a more pronounced effect than the sole addition of MK or hybrid MK-GGBFS. This

Table 3
Non-combustibility test results of HFMOC.

HFMOC	AS 1530.1 (2016)	ASTM E2652 (2018)	G30	M30	G15M15
Mass loss	-	≤ 50 %	40.2 %	38.4 %	37.5 %
Total duration of sustained flaming	< 5 s	< 10 s	NSF	NSF	NSF

Note: NSF: No sustained flame

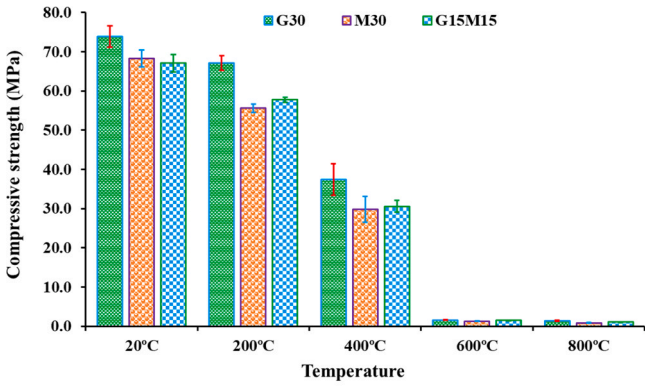

(a)

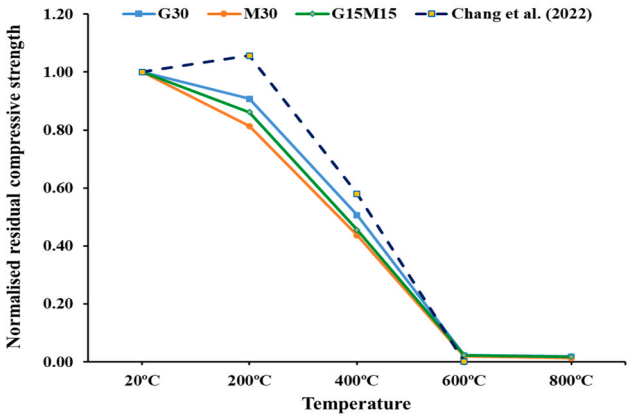

(b)

Fig. 9. (a) Compressive strength and (b) normalized residual compressive strength of HFMOC at elevated temperatures.

improvement is likely due to the filler and pozzolanic effects of GGBFS, which also enhanced fibre dispersion [54], working synergistically with phase 5 crystals to form a dense matrix, as evidenced by the morphology shown in Fig. 10.

At 200°C, the results revealed that G30 showed the maximum residual strength ratio of 0.91 with a compressive strength of 67.1 MPa, while M30 and G15M15 demonstrated strength retention ratios of 0.81 (55.6 MPa) and 0.86 (57.8 MPa), respectively. The observed reduction in compressive strength may be attributed to the melting of PE fibre, destabilization of hydration products, and water evaporation affecting the overall matrix compactness [11]. Beyond this temperature, the strength consistently decreased. At 400°C, G30 displayed strength retention of approximately 50.6 %, followed by G15M15 (45.6 %) and M30 (43.7 %), and this might be credited to the synergistic effects of brucite and BF within the matrix. As the temperature increased to 600°C and 800°C, a substantial drop in compressive strength was recorded, ranging between 0.8 and 1.5 MPa. This decline may be attributed to the breakdown of hydrated crystals, such as phase 5 and brucite, leading to a decomposed matrix with weakened bonding among the constituents, including BF, as illustrated in Fig. 11. Thus, the contribution of BF to strength retention at elevated temperatures was not significant. Similar observations were reported by Chang et al. [23] and Rawat et al. [11], who noted a complete loss in compressive strength occurring at 600°C, attributing it to the formation of a loose, powdery matrix resulting from the conversion of hydrated crystals to MgO. Unlike MOC, OPC-based composites exhibit a more gradual performance loss with increasing temperatures [27]. In OPC-based composites, dehydration of bound

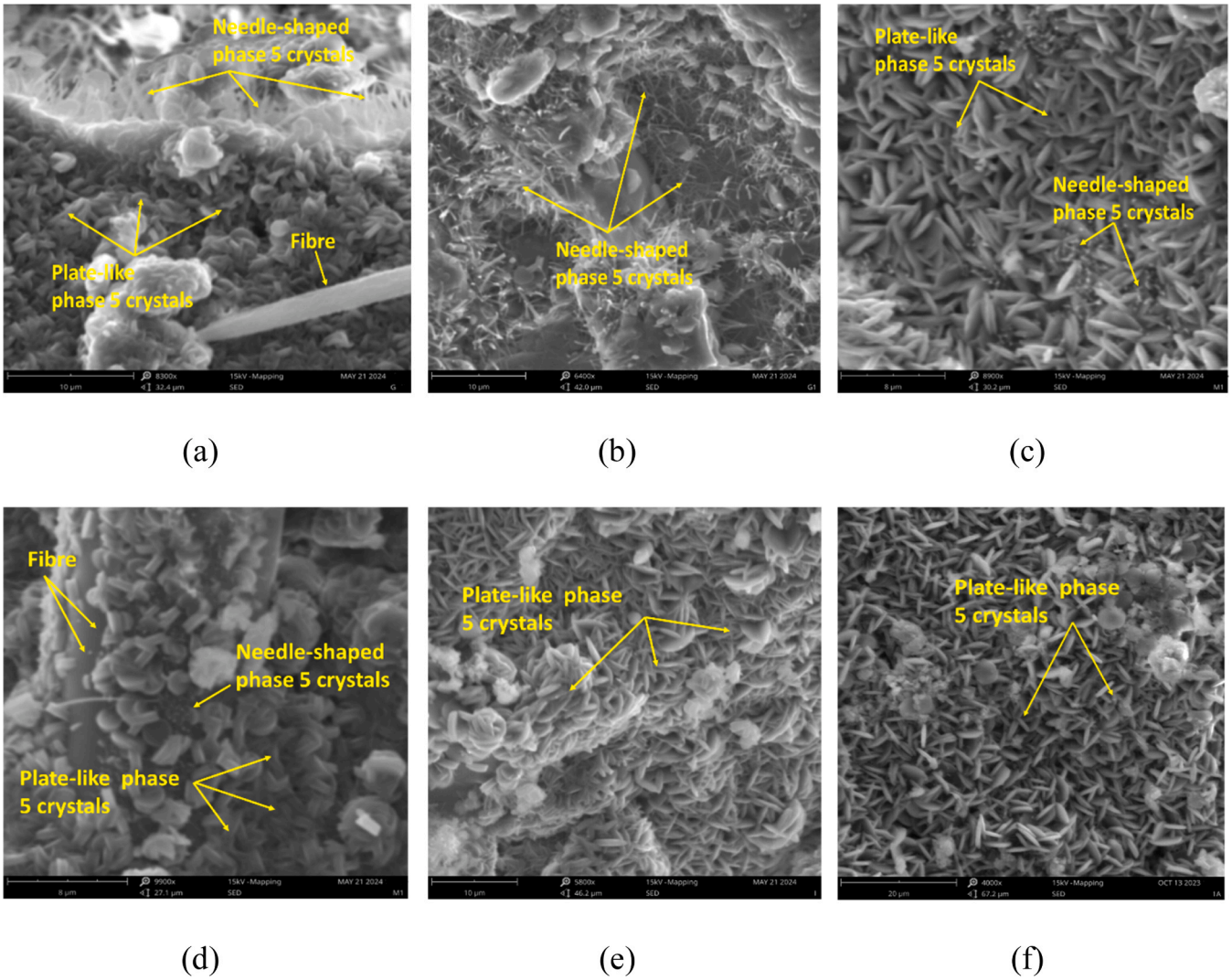

Fig. 10. Morphology of G30 (a and b), M30 (c and d), and G15M15 (e and f) at room temperature.

water in calcium silicate hydrate (C-S-H) gel begins during the initial temperature rise, followed by the decomposition of calcium hydroxide between 450–500°C. Above 700°C, the residual C-S-H phases lose their binding capacity, while thermal expansion induces microstructural cracking. This progressive degradation allows OPC to retain more residual strength at high temperatures compared to MOC [27,55]. Overall, the G30 mix exhibited excellent residual compressive strength across all temperature ranges. Moreover, the substantial loss in compressive strength at higher temperatures raises serious concerns regarding its suitability for structural applications.

The variation in compressive strength of 28-day cured HFMOC was evident from the morphology of the matrices at both room temperature and various elevated temperatures, as shown in Figs. 10 and 11. The morphology in Fig. 10 depicts the presence of needle or plate-shaped phase 5 crystals, which are primarily responsible for strength development in MOC composites [56]. These crystals establish excellent bonding with fibres (Fig. 10d), resulting in a robust fibre-matrix network synergistically contributing to higher strength at room temperature. Fig. 10 also reveals that the G30 morphology mainly consists of needle-shaped phase 5 crystals with minimal plate-like crystals, forming a dense matrix and significantly enhancing strength development. In contrast, the M30 morphology shows a high quantity of thick and short plate-like phase 5 crystals, with fewer needle-like crystals, leading to a compact matrix, though the interlocking is not as pronounced as in G30. The G15M15 matrix predominantly features short-dimension plate-like crystals, leading to less effective interlocking of crystals compared to G30 and M30, indicating the dilution effect of the hybrid admixtures in the HFMOC, resulting in a weaker matrix and reduced strength [52].

Fig. 11 illustrates the variation in matrix morphology of HFMOC with increasing temperatures. At 200°C, the micrographs illustrate a slight change in the morphology of the HFMOC matrices, highlighting effective bonding between the matrix and BF at the ITZ. Specifically, G30 exhibits an abundance of thinner, needle-like fibrous crystals surrounding the fibres, which likely contributes to its enhanced strength retention compared to M30 and G15M15. In contrast, M30 and G15M15 show shorter or even lost plate-like crystals, resulting in a decline in strength relative to G30. Additionally, the SEM images (Fig. 12) highlight grooves in the matrix caused by the melting of PE fibres, which may have facilitated the release of bound water, reducing internal pressure and mitigating spalling. At 400°C, phase 5 crystals disappear, leading to a significant drop in compressive strength (43.7–50.6 %), although the matrix maintains compactness and BF bonding at the ITZ, possibly due to brucite presence (Fig. 11 (d to f)). After the calcination temperatures of 600°C and 800°C, the matrix completely degraded, leading to a porous ITZ, as seen from the micrographs. All hydrated crystals decompose and convert to unhydrated MgO (light white color), resulting in a loose matrix that might justify the inferior strength retention [11, 23]. Additionally, the presence of BF shows no significant role in

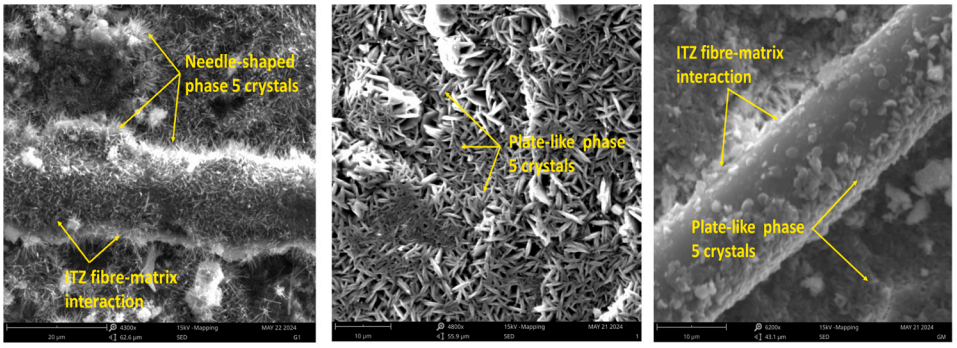

(a) G30-200ºC (b) M30-200ºC (c) G15M15-200ºC

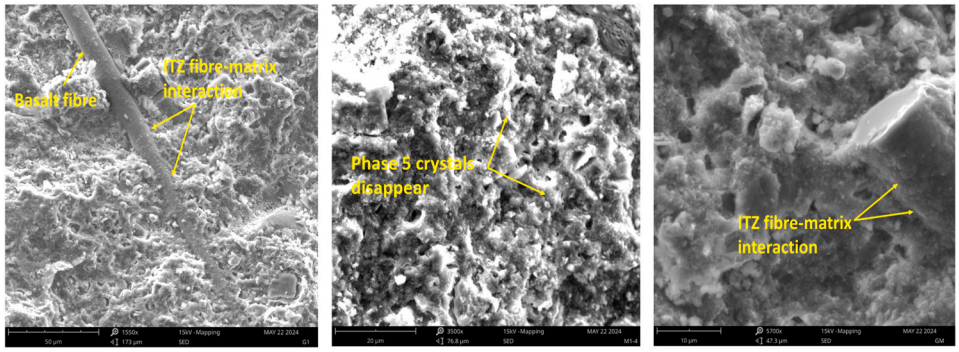

(d) G30-400ºC (e) M30-400ºC (f) G15M15-400ºC

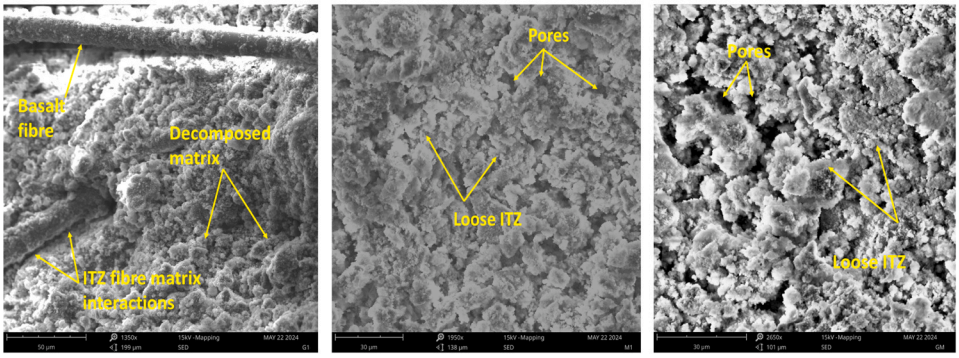

(g) G30-600ºC (h) M30-600ºC (i) G15M15-600ºC

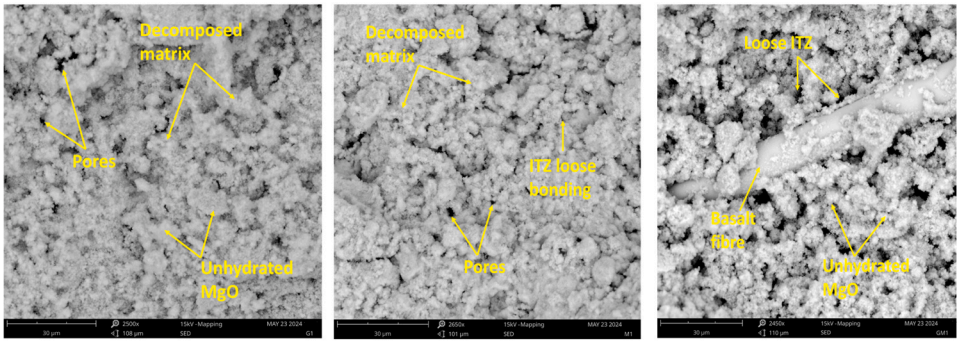

(j) G30-800ºC (k) M30-800ºC (l) G15M15-800ºC

Fig. 11. Morphology of G30, M30, and G15M15 at different temperatures.

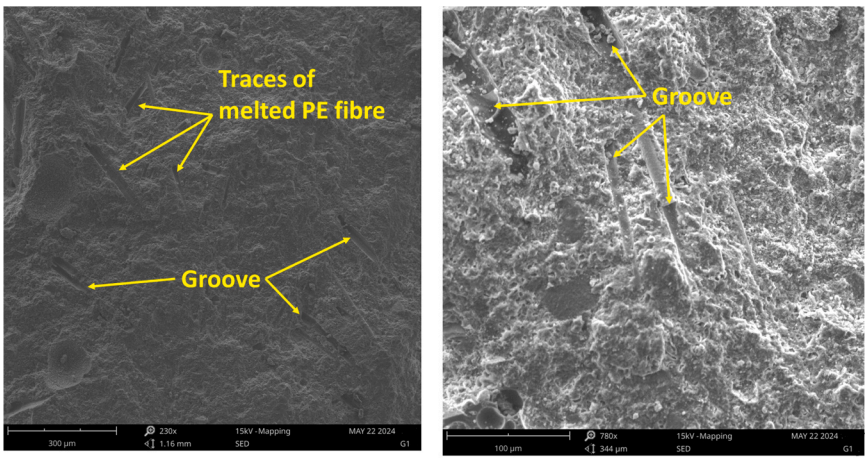

Fig. 12. (a-b) SEM images of G30 exposed to 200ºC showing traces of melted PE fibre.

strength retention at high temperatures, possibly due to the observed loose fibre-matrix interaction at the ITZ level in Fig. 11 (g to l).

The thermal degradation mechanism evident from the morphological analysis was further confirmed by the DSC analysis, as illustrated in Fig. 13. The DSC curves display distinct peaks at 159°C, 349°C, and 444°C, correlating with the progressive decomposition of hydrated phases as temperature increases. The degradation of the HFMOC matrix begins with the rise in temperature and continues steadily. Phase 5, which is the main hydration phase contributing to the strength of the HFMOC matrix at ambient conditions [18], undergoes gradual decomposition as evidenced by the consistent decline in compressive strength with increasing temperature. The stepwise decomposition of phase 5, as described in Eq. 2–6 in Section 4.2, highlights its role in strength reduction and moisture loss. The peak at 159°C is attributed to the degradation of phase 5 crystals with the loss of crystalline water. Notably, G30 exhibited a higher peak intensity than other composites, indicating a greater concentration of phase 5 crystals, which resulted in significant mass loss (Section 4.2.). This abundance of phase 5 in G30 likely contributes to its superior mechanical performance.

Additionally, the peak at 349°C corresponds to the decomposition of brucite ($Mg(OH)_2$) with the release of hydroxyl ions (OH^-) followed by the release of hydrochloric acid (HCl) gas at 444°C resulting in the regeneration of MgO (typical by-product at this temperature). The findings reveal that the decomposition and dehydration of hydration products complete before 500°C, with no significant peaks observed beyond this temperature. Overall, the morphological and DSC analyses suggest that the absence of main hydration phases at elevated temperatures is responsible for the substantial loss in compressive strength.

4.4.2. *Tensile performance of HFMOC*

Fig. 14 illustrates the normalized residual tensile strength of HFMOC at different temperatures, showing a declining trend with increasing temperatures. A drastic reduction in residual tensile strength was observed as the temperature increased from 20 to 200ºC, with a 46–66 % decrease noted at 200ºC, and G30 exhibiting the least reduction. This substantial reduction highlights the critical role of fibres and matrices in providing tensile strength, partly due to the melting of PE fibres (melting point~150ºC), and partly due to the degradation of hydration products and water evaporation [11,14]. Similar to the compressive strength findings, G30 showed an enhanced residual tensile strength ratio of 0.53, followed by M30 (0.47) and G15M15 (0.33) at 200ºC, indicating that GGBFS incorporation facilitates hydration products from significant degradation and maintains a compact matrix, as evidenced by the abundant presence of needle-shaped phase 5 crystals shown in Fig. 11 (a). As temperature rises to 400ºC, the decline in tensile strength intensifies to 72–87 %, primarily due to the complete degradation of phase 5 crystals. However, the presence of brucite crystals and BF provides some residual support to the matrix structure. Beyond 400ºC, a complete loss of tensile strength occurs due to the decomposition of hydration products into MgO, resulting in a porous and powdery matrix.

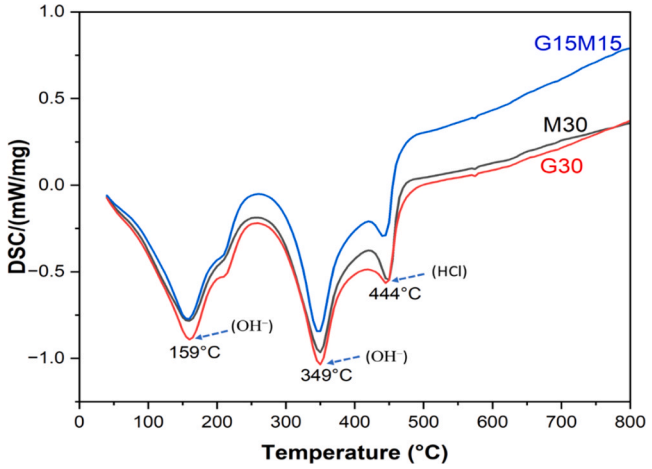

Fig. 13. DSC curves of HFMOC at varying temperatures.

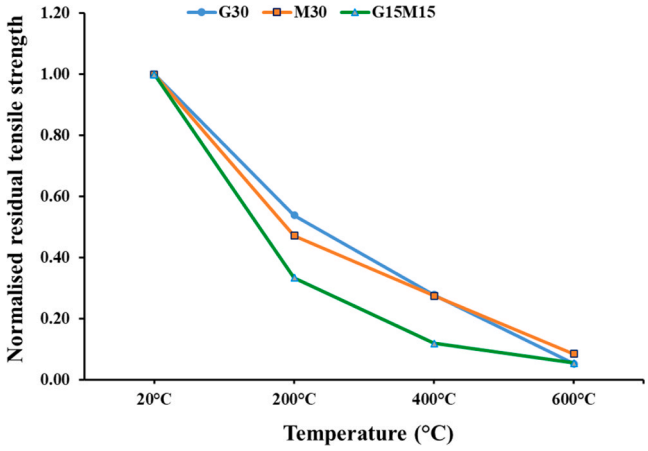

Fig. 14. Normalised residual tensile strength of HFMOC.

4.4.2.1. Tensile stress-strain behaviour of HFMOC. Fig. 15 presents the typical tensile stress-strain curves of HFMOC calcined at temperatures ranging from 20ºC to 600ºC. At room temperature, all HFMOC specimens exhibited ductile failure with strain-hardening behaviour, reaching ultimate tensile stress before transitioning to strain-softening. Among them, G30 displayed the most robust strain-hardening performance, followed by M30 and G15M15. However, as the temperature increased to 200ºC and 400ºC, the ductile failure characteristic disappeared, giving way to brittle failure immediately after the elastic limit. At 600ºC, a significant reduction in tensile strength was observed, with the stress-strain curve showing a flatter slope before failure, indicating a marked loss in material toughness.

Among HFMOC, G30 showed an enhanced strain capacity of 2.22 % followed by M30 (1.83 %), and G15M15 (1.43 %) at room temperature. The improved strain capacity of G30, followed by M30 and G15M15, may be attributed to the uniform dispersion of fibres and suitable bonding of PE fibres with the MOC matrix, which facilitates multiple cracking behaviours [14,54,57]. Regarding tensile strength, G15M15 achieved the highest value at 8.58 MPa, followed by G30 at 8.37 MPa and M30 at 7.64 MPa, resulting in an overall tensile strength range of 7.64–8.58 MPa for the HFMOC composites. These values significantly surpass those reported by Wei et al. [57] (5 MPa) and Wang et al. [58] (7 MPa) for MOC composites reinforced with 2 % PE fibre, suggesting that incorporating hybrid fibres likely contributes to this improved tensile strength, as recommended by Ahmad et al. [18]. At 200ºC, all HFMOC specimens experienced a complete loss of strain capacity, as shown in Fig. 15, although a significant portion of tensile strength was retained. The loss in strain capacity is primarily attributed to the melting of PE fibres, which are responsible for imparting ductility to MOC composites [14]. Despite this, HFMOC composites retained considerable tensile strength at 200ºC, with values of 4.51 MPa for G30, 3.61 MPa for M30, and 2.87 MPa for G15M15, likely due to the presence of BF and phase 5 crystals within the matrices. A similar stress-strain pattern was observed at 400ºC, with tensile strengths of 2.33, 2.1, and 1.03 MPa for G30, M30, and G15M15, respectively. However, at 600ºC, tensile strength retention was nearly negligible, ranging from 0.44 to 0.65 MPa, which can be attributed to the complete degradation of hydration products and the regeneration of light white MgO as a by-product, resulting in a porous ITZ. Despite the presence of BF in the matrix, it did not contribute significantly to strength retention, possibly due to the weak fibre-matrix interaction. Overall, G30 containing 30 % GGBFS exhibited excellent tensile strength retention at ambient temperature, 200ºC, and 400ºC, likely due to GGBFS's ability to maintain a dense matrix and protect hydration products from significant degradation.

4.5. XRD analysis of HFMOC

Fig. 16 (a-c) illustrates the variations in phase compositions for

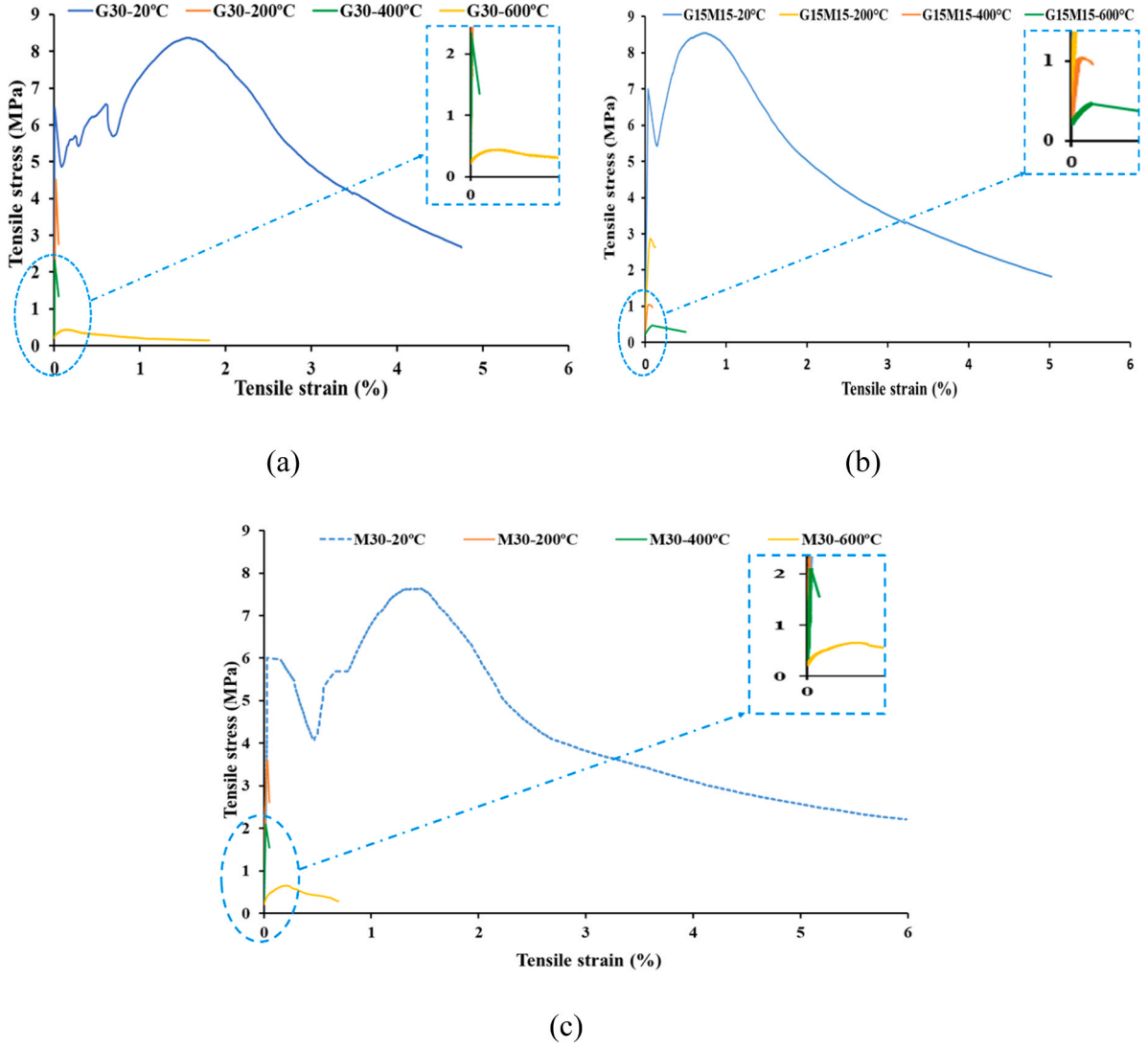

Fig. 15. Typical tensile stress-strain curves of HFMOC.

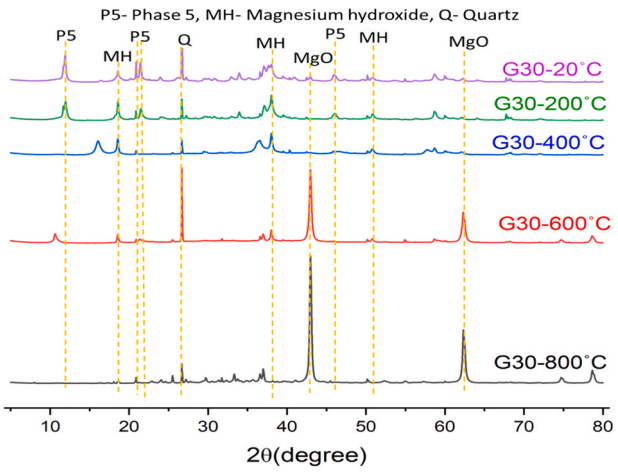

(a)

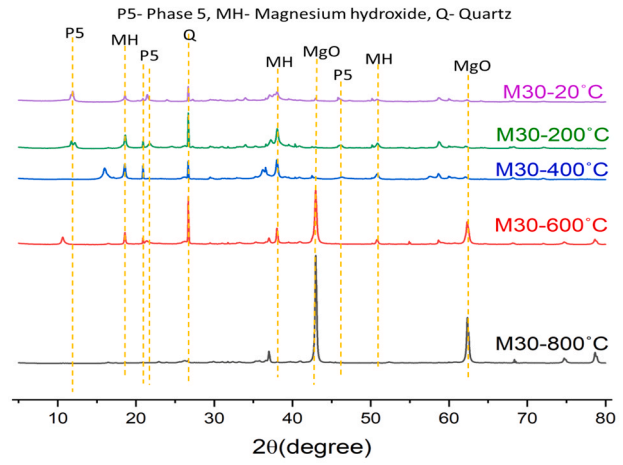

(b)

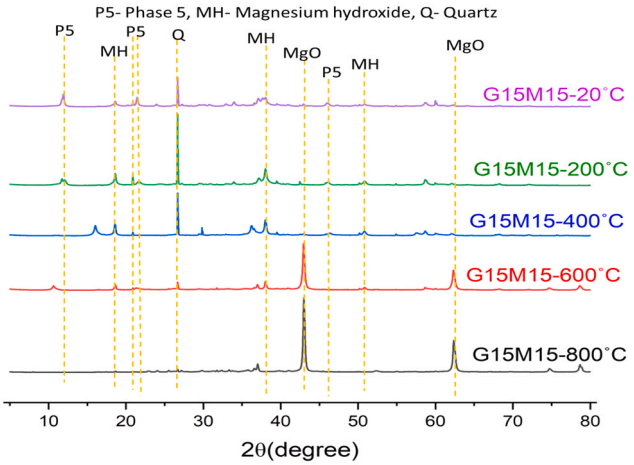

(c)

Fig. 16. XRD analysis of HFMOC at different temperatures.

HFMOC specimens subjected to elevated temperatures. The patterns reveal that significant transformations occur in the crystalline phases as the temperature increases. Certain phases that are abundant at lower temperatures either disappear or transform into different phases as the temperature rises, while others emerge. These changes are linked to the thermal stability of the hydration products. Notably, Phase 5 crystals, abundant in each mix at ambient temperature, gradually diminish at 200ºC and completely disappear at temperatures exceeding 200ºC. Similarly, brucite ($Mg(OH)_2$), present up to 400ºC, transforms into MgO beyond this temperature. The regeneration of substantial amounts of MgO (a typical byproduct at 600ºC and 800ºC) led to a significant reduction in mechanical properties [11]. The XRD analysis provides a detailed understanding of the thermal degradation mechanism of HFMOC matrices, which aligns with the morphological variations observed in Figs. 10 and 11.

In the HFMOC mixes, various crystalline phases such as phase 5, $Mg(OH)_2$, quartz, and unreacted MgO were identified at ambient temperature. Among these, phase 5 and $Mg(OH)_2$ are recognized as the primary hydration products of HFMOC, with phase 5 being the main contributor to strength development [18]. The presence of MgO indicates unreacted MgO, while the quartz content is due to the inclusion of SCMs and sand. The analysis showed an abundant presence of phase 5 in the mixes, with its diffraction peaks observed at approximately 12°, 21.5°, 20.9°, and 46.1° 2θ. $Mg(OH)_2$ peaks appeared at 18.6°, 38.1°, and 50.9° 2θ, while MgO peaks were detected at around 42.9° and 62.4° 2θ. Notably, the G30 mix exhibited the highest peak intensity for phase 5 at 12°, 20.9°, and 21.5° 2θ at ambient temperature, indicating that the inclusion of 30 % GGBFS effectively enhances the formation of phase 5 crystals, leading to superior strength compared to other HFMOC specimens. As the temperature increased to 200ºC, a reduction in phase 5 peak intensity was observed, although G30 showed minimal reduction, suggesting better strength retention compared to M30 and G15M15. Beyond 200ºC, phase 5 diffraction peaks disappeared, with $Mg(OH)_2$ and MgO phases becoming prominent at 400ºC. The increased $Mg(OH)_2$ content at this temperature contributed to strength retention and matrix integrity, as indicated by the morphological analysis. Beyond 400°C, $Mg(OH)_2$ peaks decreased significantly and disappeared completely at 800°C. In contrast, MgO peaks intensified at 600ºC and surged at 800ºC, attributed to the degradation of hydrated products into MgO. This transformation led to a substantial loss in mechanical strength at higher temperatures (600ºC and 800ºC), primarily due to the regeneration of MgO, which resulted in a weak and porous ITZ, as evidenced by the morphological analysis in Fig. 11 (g to l).

5. Conclusion

The fire resistance and thermal performance of HFMOC reinforced with hybrid PE and BF fibres, GGBFS, MK, and a hybrid of GGBFS-MK have been assessed for its suitability for non-structural and structural applications. For this purpose, both macro-scale and micro-scale analyses of HFMOC at elevated temperatures were conducted to uncover the underlying mechanisms. Based on the comprehensive experimental findings, the following conclusions are drawn:

- HFMOC specimens exhibited substantial mass loss with increasing temperature, ranging from 34–35.4 % at 600°C to 36–38.1 % at 800°C, exceeding that of OPC-based composites. This higher mass loss indicates HFMOC's effectiveness in fire suppression through moisture release, supporting its potential for fire mitigation applications.
- The thermal conductivity of HFMOC specimens G30, M30, and G15M15 ranged from 1.30–0.14 W/(m.K), 1.19–0.17 W/(m.K), and 1.16–0.19 W/(m.K), respectively, over a temperature range of 20–500°C. Among these, G30 demonstrated the most pronounced reduction in thermal conductivity with increasing temperature.
- The non-combustibility analysis verified that all developed HFMOC mixes were non-combustible and non-flammable, with no sustained flaming observed. The recorded mass loss ranged from 37.5 % to 40.2 %, remaining well below the allowable threshold of 50 %.

- Visual inspection revealed that the HFMOCs exhibited no spalling and only minor cracking over the temperature range of 200–800°C. This improved spalling resistance is attributed to the melting of PE fibres facilitating the release of entrapped vapor pressure. The enhanced spalling resistance and non-combustible nature of HFMOC specimens at elevated temperatures highlight the potential of MOC for non-structural applications such as cladding, facades, and flooring, where strength retention is not the primary concern.
- The developed HFMOC exhibited excellent mechanical performance and strain hardening behaviour at room temperature with G30 containing 30 % GGBFS exhibiting excellent compressive strength (73.9 MPa), tensile strength (8.37 MPa), and strain capability (2.22 %). This enhanced performance was attributed to the presence of GGBFS which facilitates the formation of phase 5 and uniform fibre dispersion.
- The compressive strength of HFMOC significantly decreased with increasing temperature, with losses ranging from 9.20 % to 18.6 % at 200°C and 49.4–54.4 % at 400°C, followed by an almost complete reduction (~98 %) at 600°C and 800°C. Among the mixes, G30 exhibited the least reduction in compressive strength, with 9.20 % and 49.4 % losses at 200°C and 400°C, respectively. The severe strength reduction at elevated temperatures highlights the limitations of HFMOC for structural applications.
- The tensile strength of HFMOC also decreased significantly with increasing temperature, with reductions of approximately 46.1 %–66.6 % at 200°C, 72.1 %–87.9 % at 400°C, and 91.5 %–94.7 % at 600°C. The drastic reduction at 200°C was primarily due to the melting of PE fibre considered mainly responsible for tensile strength and strain hardening in HFMOC.
- Morphological analysis showed significant matrix degradation with increasing temperature. Phase 5, a key contributor to strength at room temperature, gradually degraded up to 200°C and completely disappeared beyond this point, leading to a porous and powdery ITZ at higher temperatures. This degradation likely contributed to the significant loss in strength. These morphological changes were verified by DSC and XRD analysis, which detailed the phase transformations at each temperature.
- DSC and XRD analyses provided further insight into the degradation mechanism, showing that the decomposition of phase 5 was completed below 500°C, primarily converting into MgO at elevated temperatures. This transformation led to significant mass loss and a notable reduction in strength.

CRediT authorship contribution statement

Zhang Y.X.: Writing – review & editing, Supervision, Resources, Project administration, Methodology, Funding acquisition, Conceptualization. **Zhang Lihai:** Writing – review & editing, Supervision, Methodology, Funding acquisition. **Yang Chunhui:** Writing – review & editing, Supervision, Resources. **Rawat Sanket:** Writing – review & editing, Supervision, Methodology, Investigation, Conceptualization. **Ahmad Farhan:** Writing – original draft, Validation, Methodology, Investigation, Formal analysis, Data curation, Conceptualization.

Declaration of Competing Interest

The authors declare that they have no known competing financial interests or personal relationships that could have appeared to influence the work reported in this paper.

Acknowledgments

The support of the Australian Research Council Discovery Project (DP220103043) and the School of Engineering, Design and Built Environment, Western Sydney University is gratefully acknowledged. The authors would also like to acknowledge Dr. Daniel Fanna, Dr. Laurel George and Dr. Richard Wuhrer from the Advanced Materials Characterisation Facility (AMCF), Western Sydney University for access to instrumentation and training.

Data availability

Data will be made available on request.

References

[1] L. Soufeiani, et al., Fire safety performance of 3D GFRP nanocomposite as a cladding material, Fire Saf. J. 133 (2022) 103670.
[2] Environmental Planning and Assessment Amendment (Identification of Buildings with External Combustible Cladding) Regulation. The Environmental Planning and Assessment Act 1979. 7. 2018. Available online: ⟨https://legislation.nsw.gov.au/view/pdf/asmade/sl-2018-499⟩ (accessed on 14 December 2023).
[3] Department of Housing and Public Works Queensland Government. Guideline – for assessing buildings with combustion cladding (2019), pp. 1-58 ⟨http://www.hpw.qld.gov.au/SiteCollectionDocuments/GuidelineAccessCombustibleBuildings⟩.pdf'.
[4] R. Watermeyer, K. Strydom, The fire safety performance of internal and external walls in multi-storey buildings, Civ. Eng. = Siviele Ing. 2020 (2) (2020) 28–31.
[5] J. Pancheti, M. Mahendran, E. Steau, Fire resistance of external LSF walls with corrugated steel cladding, J. Constr. Steel Res. 188 (2022) 107008.
[6] E.K. Asimakopoulou, D.I. Kolaitis, M.A. Founti, Thermal characteristics of externally venting flames and their effect on the exposed façade surface, Fire Saf. J. 91 (2017) 451–460.
[7] M.S. McLaggan, et al., Flammability trends for a comprehensive array of cladding materials, Fire Saf. J. 120 (2021) 103133.
[8] T. Thevega, et al., Fire compliance of construction materials for building claddings: A critical review, Constr. Build. Mater. 361 (2022) 129582.
[9] T. Singh, D. Page, I. Simpson, Manufactured structural timber building materials and their durability, Constr. Build. Mater. 217 (2019) 84–92.
[10] H.T. Mohan, K. Jayanarayanan, K. Mini, Recent trends in utilization of plastics waste composites as construction materials, Constr. Build. Mater. 271 (2021) 121520.
[11] S. Rawat, et al., Mechanical Performance of Hybrid Fibre Reinforced Magnesium Oxychloride Cement-Based Composites at Ambient and Elevated Temperature, Buildings 14 (1) (2024) 270.
[12] Y. Xie, et al., Mechanical performance and water resistance of biochar admixture lightweight magnesium oxychloride cement, Sci. Total Environ. 912 (2024) 168773.
[13] Z.-h He, et al., Upcycling textile sludge into magnesium oxychloride cement: physical properties, microstructure, and leaching behavior, Sci. Total Environ. 924 (2024) 171416.
[14] K. Yu, et al., Magnesium oxychloride cement-based strain-hardening cementitious composite: mechanical property and water resistance, Constr. Build. Mater. 261 (2020) 119970.
[15] F. Ahmad, et al., Effect of metakaolin and ground granulated blast furnace slag on the performance of hybrid fibre-reinforced magnesium oxychloride cement-based composites, Int. J. Civ. Eng. (2025) 1–16.
[16] Y. Guo, Y. Zhang, K. Soe, Effect of sodium monofluorophosphate and phosphates on mechanical properties and water resistance of magnesium oxychloride cement, Cem. Concr. Compos. 129 (2022) 104472.
[17] Y. Guo, et al., Development of magnesium oxychloride cement with enhanced water resistance by adding silica fume and hybrid fly ash-silica fume, J. Clean. Prod. 313 (2021) 127682.
[18] F. Ahmad, et al., Effect of hybrid fibres on mechanical behaviour of magnesium oxychloride cement-based composites, Constr. Build. Mater. 424 (2024) 135937.
[19] F. Ahmad, S. Rawat, Y. Zhang, Magnesium oxychloride cement: development, opportunities and challenges, Appl. Sci. 14 (7) (2024) 3074.
[20] S.A. Walling, J.L. Provis, Magnesia-based cements: a journey of 150 years, and cements for the future? Chem. Rev. 116 (7) (2016) 4170–4204.
[21] Montle, J. and K.G. Mayhan, The role of magnesium oxychloride as a fire-resistive material. 1974.
[22] Thompson, H., Magnesium oxychloride fireproofing. 1973, Google Patents.
[23] C. Chang, et al., Effect of calcination temperature on mechanical properties of magnesium oxychloride cement, Materials 15 (2) (2022) 607.
[24] S. Rawat, F.A. Khin Soe, Lihai Zhang, Y.X. Zhang, Magnesium oxychloride cement-based composites: unveiling fire resistance for structural and non-structural applications, Int. Conf. Fire Saf. Eng. Res. Pract. (iCFSERP 2024 (2024).
[25] Ahmad, F., et al. Effect of temperature on compressive behaviour of hybrid fibre-reinforced magnesium oxychloride cement-based composites. in Australasian Structural Engineering Conference 2024 (ASEC 2024): Structural Engineering for a Sustainable Future. 2024. Engineers Australia Melbourne.
[26] C.-S. Poon, et al., Performance of metakaolin concrete at elevated temperatures, Cem. Concr. Compos. 25 (1) (2003) 83–89.
[27] S. Rawat, C. Lee, Y. Zhang, Performance of fibre-reinforced cementitious composites at elevated temperatures: A review, Constr. Build. Mater. 292 (2021) 123382.
[28] P. Sullivan, R. Sharshar, The performance of concrete at elevated temperatures (as measured by the reduction in compressive strength), Fire Technol. 28 (1992) 240–250.

[29] S. Rawat, et al., Development of sustainable engineered cementitious composite with enhanced compressive performance at elevated temperatures using high volume GGBFS, J. Clean. Prod. 451 (2024) 142011.
[30] X. Yigang, et al., Residual properties of PFA concrete subjected to high temperatures, Proc. Int. Symp. . High. Perform. Concr. (2000).
[31] A. Danish, et al., Hope or hype? Evaluating the environmental footprint of reclaimed fly ash in geopolymer production, Resour., Conserv. Recycl. 205 (2024) 107564.
[32] N. Abdelmelek, et al., Effect of elevated temperatures on microstructure of high strength concrete based-metakaolin, J. King Saud. Univ. -Eng. Sci. (2021).
[33] A. Albidah, et al., Behavior of metakaolin-based geopolymer concrete at ambient and elevated temperatures, Constr. Build. Mater. 317 (2022) 125910.
[34] N. Abdelmelek, E. Lubloy, Evaluation of the mechanical properties of high-strength cement paste at elevated temperatures using metakaolin, J. Therm. Anal. Calorim. 145 (2021) 2891–2905.
[35] H. Alghamdi, et al., Enhanced mechanical, thermal and fire resistance performance of expanded polystyrene-based fiber-reinforced mortar made with limestone-calcined clay cement (LC3), Innov. Infrastruct. Solut. 8 (10) (2023) 265.
[36] M. Khan, et al., Experimental and analytical study of hybrid fiber reinforced concrete prepared with basalt fiber under high temperature, Fire Mater. 46 (1) (2022) 205–226.
[37] A. Alaskar, et al., Performance evaluation of high-strength concrete reinforced with basalt fibers exposed to elevated temperatures, J. Build. Eng. 35 (2021) 102108.
[38] Y. Guo, UNSW Sydney, Dev. Water-Resist. Magnes. Oxychloride Cem. (2020).
[39] Standards Australia AS 1530.1:2024 Methods for Fire Tests on Building Materials, Components and Structures - Combustibility Test for Materials.
[40] A.H. Akca, N.Ö. Zihnioğlu, High performance concrete under elevated temperatures, Constr. Build. Mater. 44 (2013) 317–328.
[41] K. Li, et al., Intrinsically hydrophobic magnesium oxychloride cement foam for thermal insulation material, Constr. Build. Mater. 288 (2021) 123129.
[42] T.S. Yun, et al., Evaluation of thermal conductivity for thermally insulated concretes, Energy Build. 61 (2013) 125–132.
[43] A. Sales, et al., Lightweight composite concrete produced with water treatment sludge and sawdust: Thermal properties and potential application, Constr. Build. Mater. 24 (12) (2010) 2446–2453.
[44] K.-H. Kim, et al., An experimental study on thermal conductivity of concrete, Cem. Concr. Res. 33 (3) (2003) 363–371.
[45] K.-Y. Shin, et al., Thermo-physical properties and transient heat transfer of concrete at elevated temperatures, Nucl. Eng. Des. 212 (1-3) (2002) 233–241.
[46] A. Eddhahak-Ouni, et al., Experimental and multi-scale analysis of the thermal properties of Portland cement concretes embedded with microencapsulated Phase Change Materials (PCMs), Appl. Therm. Eng. 64 (1-2) (2014) 32–39.
[47] B. Xu, et al., Influence of cenospheres on properties of magnesium oxychloride cement-based composites, Mater. Struct. 49 (2016) 1319–1326.
[48] M. Yu, et al., Experimental and numerical investigation on thermal properties of alkali-activated concrete at elevated temperatures, J. Build. Eng. 74 (2023) 106924.
[49] P. He, et al., Mechanical, durability and environmental aspects of magnesium oxychloride cement boards incorporating waste wood, J. Clean. Prod. 207 (2019) 391–399.
[50] J.C. Mendes, et al., On the relationship between morphology and thermal conductivity of cement-based composites, Cem. Concr. Compos. 104 (2019) 103365.
[51] . ASTM E2652-18 Standard Test Method for Assessing Combustibility of Materials Using a Tube Furnace with a Cone-Shaped Airflow Stabilizer (2018) at 750°C. West Conshohocken, Pennsylvania, USA.
[52] W. Gong, N. Wang, N. Zhang, Effect of fly ash and metakaolin on the macroscopic and microscopic characterizations of magnesium oxychloride cement, Constr. Build. Mater. 267 (2021) 120957.
[53] N. Zhang, et al., Effects of fly ash and slag on the properties of magnesium oxysulfate cement, Emerg. Mater. Res. 8 (3) (2019) 472–482.
[54] Y. Zhu, Y. Yang, Y. Yao, Use of slag to improve mechanical properties of engineered cementitious composites (ECCs) with high volumes of fly ash, Constr. Build. Mater. 36 (2012) 1076–1081.
[55] H. Song, et al., A study of thermal decomposition of phases in cementitious systems using HT-XRD and TG, Constr. Build. Mater. 169 (2018) 648–661.
[56] Y. Nie, et al., Mechanical, water resistance and environmental benefits of magnesium oxychloride cement incorporating rice husk ash, Sci. Total Environ. 849 (2022) 157871.
[57] L. Wei, et al., Feasibility study of strain hardening magnesium oxychloride cement-based composites, Constr. Build. Mater. 165 (2018) 750–760.
[58] Y. Wang, et al., Mechanical properties of high ductile magnesium oxychloride cement-based composites after water soaking, Cem. Concr. Compos. 97 (2019) 248–258.